Tracking atmospheric water pathways by direct evaporation tagging: A case study for West Africa

Hans Richard Knoche[1] and Harald Kunstmann[1,2]

Received 7 April 2013; revised 17 October 2013; accepted 21 October 2013; published 20 November 2013.

[1] One of the central questions in hydrological research is where and to what extent evaporated water of a region returns as precipitation in another region. This study addresses this question and presents a detailed process-based approach implemented into a regional climate model. It allows tagging and tracking of the moisture evaporating from a given region into the atmosphere until it returns to the land surface as precipitation. Our approach is fully three-dimensional and enables the detailed consideration of vertical transport mechanisms for tagged water. We present a case study for the region around Lake Volta in West Africa. The simulation demonstrates the performance of the regional model and the implemented tagging mechanism. It shows the evolution of the tagged moisture field and reveals details of the transport: Moisture evaporated from Lake Volta is initially transported predominantly to the east and north, lifted by convective processes and then transported in upper layers to the west far away from the source of evaporation. The results indicate that the coupling between boundary layer and higher levels through convective processes can be essential for the fate of tagged water substances. Detailed analysis for a 2 month period in the rainy season 1998 shows that locally up to 6% of precipitating water originates from the Lake Volta region. Less than 2% of the evaporated water is locally recycled as precipitation in the source area. A further 10% precipitates in the rest of the Volta Basin.

Citation: Knoche, H. R., and H. Kunstmann (2013), Tracking atmospheric water pathways by direct evaporation tagging: A case study for West Africa, *J. Geophys. Res. Atmos.*, *118*, 12,345–12,358, doi:10.1002/2013JD019976.

1. Introduction

[2] The hydrological cycle plays a crucial role in the Earth's climate system. To understand in more detail how the terrestrial and atmospheric water cycle compartments are interlinked at the land surface, it has to be investigated what happens to water vapor after evaporation from the surface and where it finally precipitates and enters again the terrestrial compartment [*Eltahir and Bras*, 1996].

[3] To assess the relevance of evaporated water for subsequent precipitation, the concept of regional moisture recycling is used [e.g., *Eltahir and Bras*, 1996; *Savenije*, 1995]. It relates the water vapor evaporating from a given source area to the precipitating water in the same region or, more generally, in an arbitrary target area. The magnitude of the contribution of recycled water to a region's precipitation is an indicator of the importance of land surface processes in the water balance of a region and is often interpreted as an indicator of general climatic sensitivity to land surface change [*Brubaker et al.*, 1993]. An extensive overview of the distribution of atmospheric moisture and the methods used to identify sources and sinks is given by *Gimeno et al.* [2012].

[4] In many earlier studies, comparatively simple model formulations were applied to investigate precipitation recycling. These so-called bulk models [e.g., *Brubaker et al.*, 1993; *Eltahir and Bras*, 1994; *Trenberth*, 1999; *Burde and Zangvil*, 2001] are based on various simplifying assumptions. The most restrictive assumption usually is the premise of a perfectly mixed atmosphere. More recently, process-based Lagrangian or Eulerian approaches were also applied to address water-recycling investigations. Lagrangian (trajectory) analyses, for example, determine pathways of moisture parcels and can identify the moisture sources of precipitation [e.g., *Dirmeyer and Brubaker*, 1999; *James et al.*, 2004; *Stohl and James*, 2004; *Sodemann et al.*, 2008]. Using the Eulerian methods, the moisture evaporating from any given region can be traced, and the recycled share of precipitation can be calculated, in principle.

[5] Eulerian tracing models are applied with different degrees of accuracy and detail. Off-line models, for example, calculate the fate of moisture using wind fields and

[1]Karlsruhe Institute of Technology, Institute for Meteorology and Climate Research, Garmisch-Partenkirchen, Germany.
[2]University of Augsburg, Institute of Geography, Augsburg, Germany.

Corresponding author: H. R. Knoche, Karlsruhe Institute of Technology, Institute for Meteorology and Climate Research, Kreuzeckbahnstr. 19, DE 82467 Garmisch-Partenkirchen, Bavaria, Germany. (hans-richard.knoche@kit.edu)

2169-897X/13/10.1002/2013JD019976

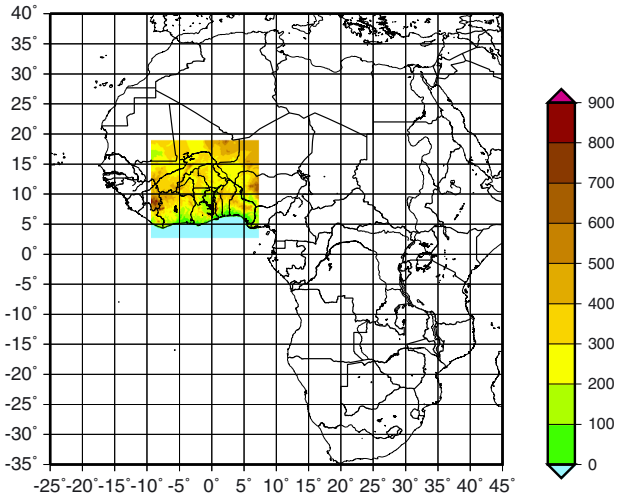

Figure 1. Location of study cite: Central West Africa.

further information from external atmospheric analyses or simulation models. They can be operated at very little computational cost, especially when the tracing problem is reduced to two spatial dimensions by assuming a well-mixed atmosphere in the vertical [e.g., *van der Ent et al.*, 2010]. In contrast, atmospheric online models with a built-in tagging mechanism are more expensive. In such extended models, the moisture originating in a specified source region is tagged and treated as an additional three-dimensional moisture field. The further development of the tagged moisture in space and time, including phase transitions, is then calculated online within the simulation model.

[6] The first simplified tagging simulations were realized with global models (*Joussaume et al.* [1986] and *Koster et al.* [1986] and later, e.g., *Numaguti* [1999] and *Bosilovich and Schubert* [2002]), focusing on studies of large-scale moisture source-target relations. The first tagging simulations with a regional model were accomplished by *Sodemann* [2006] and *Sodemann et al.* [2009] in a 3 day, respectively, 8 day simulation with a horizontal resolution of about 55 km for an investigation of the moisture transport associated with a severe flood event in Central Europe.

[7] For the present study, we have implemented a detailed tagging mechanism into the *Mesoscale Meteorological* community *Model* MM5 [*Grell et al.*, 1995]. The extended model tracks the tagged moisture until it leaves the model domain or returns to the land surface as precipitation. As outlined in detail in section 2, all relevant processes like advection, mixing, and phase changes are considered and are treated in the same manner as in the original model formulation. The model is then applied with high spatial and temporal resolutions to the region around the Volta Basin in tropical West Africa (Figure 1). As source area for the tagged moisture, we define an area around Lake Volta (Ghana), the largest man-made reservoir in the world with respect to the evaporating surface (8500 km^2). It is because of this large evaporating surface area in combination with the complex Monsoon dominated flows that we assume this region as a suited case study test site.

[8] The Monsoon circulations in West Africa are forced and maintained by land-sea thermal contrasts and by latent heat released into the atmosphere [e.g., *Xue et al.*, 2010]. The monsoon develops following the seasonal northward migration of the *Intertropical Convergence Zone* (ITCZ), identifiable as zone of maximum rainfall. In this region, humid tropical maritime air masses from the Atlantic Ocean meet dry continental Saharan air along an inclined interfacial surface (*Intertropical Discontinuity*, ITD). The northernmost position of the ITCZ is reached in July and August, which causes singular rainfall maxima in these months in the northern drier parts of West Africa. Farther south, in the humid Guinea Coast region, the migration of the ITCZ results in a bimodal precipitation distribution with two rainy seasons and two dry seasons. In summer, above the monsoon winds, the *African Easterly Jet* (AEJ) forms with a maximum height around 600–700 hPa. The AEJ is the result of strong baroclinicity across the ITD, together with associated contrasts in convection (moist to the south and dry to the north) [*Lafore et al.*, 2011]. The instability of the AEJ is one of the mechanisms that favor the generation of the *African Wave Disturbances* that modulate precipitation during summer months [*Druyan and Hall*, 1996]. As shown in various regional model simulations, many of the disturbances are responsible for significant precipitation although these disturbances may not be the exclusive precipitation trigger [*Druyan et al.*, 2006]. In the last years, numerous model-based studies have been performed to further investigate the complex multiscale climatic processes in this region [e.g., *Sylla et al.*, 2010; *Paeth et al.*, 2011].

[9] The aim of this paper is to introduce the implementation and technical realization of an ET-tagging approach in a regional climate model (RCM) like MM5 and to investigate the fate of the tagged moisture in a case study for West Africa. As will be seen in the results section, the coupling between the boundary layer and higher layers with a rotated wind direction and increased horizontal wind speed can play a crucial role in the final distribution of tagged water. As we are particularly interested in the role of vertical transport, we choose a short simulation period (2 months, typically for the rainy season) and a comparatively small model domain when compared to the regions to which existing lumped approaches have been applied so far. Although the water balance effect from moisture recycling in the traditional sense seems to be of minor importance at scales up to 1000 km [*Goessling and Reick*, 2011], a highly resolved simulation for a small region allows a sharper view on the traced evaporated water and can show details of the transport not seen in simpler or more coarsely resolved models even over a larger region.

[10] Section 2 gives a brief overview of the regional model used (MM5) including its basic features, the selected model version, the chosen parameterization schemes, and the new extensions implemented here to include the evaporation tagging mechanisms. Section 3 explains the experimental design of the case study and the configuration of the model simulation. Simulation results, with evaluation and discussion, are presented in section 4, followed by summary and concluding remarks in section 5.

2. Evaporation Tagging Extension in the RCM

2.1. Selected Basic RCM MM5

[11] The model used for this study is based on the Fifth-Generation Mesoscale Model (MM5) that was developed at

the Pennsylvania State University and the National Center of Atmospheric Research (NCAR). MM5 [*Grell et al.*, 1995] is a nonhydrostatic limited-area model designed for meteorological and climatological applications at the synoptic and subsynoptic scale. It describes, among other processes, atmospheric transport, diffusive and turbulent processes, short- and long-wave radiation, phase changes of water substance, and the formation of precipitation. The model calculates time-dependent fields of wind, temperature, pressure, water vapor and liquid and ice phase cloud, and precipitation compounds. Several surface or soil-vegetation-snow submodels with different degrees of detail and complexity are also included.

[12] Horizontally, the model equations are formulated in Lambert Conformal, Polar Stereographic, or Mercator projection map coordinates. In the vertical direction, a terrain-following height coordinate is used. For all explicit model state variables, the initial values, boundary values at the atmospheric lateral domain faces, and surface or subsurface boundary values are required (at least temperatures at sea surface and at model resolved lake surfaces) and must be provided by external simulation or analysis data sets.

[13] For the treatment of atmospheric physical processes, a variety of different parameterizations and options can be chosen, allowing MM5 to be applied to different climate and dynamic conditions worldwide (see, e.g., *Kunstmann and Jung* [2007] for an investigation of the influence of land use changes on precipitation in West Africa). A detailed description of the MM5 basic features can be found in *Dudhia* [1993] and *Grell et al.* [1995].

[14] As starting point for the tagging model extension, we adopted the MM5 model version V3.5, with the following physical parameterizations: the *Rapid Radiation Transfer Model* for the atmospheric short-wave and long-wave radiation calculations [*Mlawer et al.*, 1997], the modified scheme [*Hong and Pan*, 1996] of the *Medium Range Forecast Model* of the National Centers for Environmental Prediction (NCEP) for planetary boundary layer modeling and turbulence parameterization, and the *Reisner Mixed-Phase* scheme [*Reisner et al.*, 1998] for the treatment of grid-scale resolved cloud and precipitation physics.

[15] As surface/subsurface model, we use the *Oregon State University Land Surface Model* (OSU-LSM) [*Chen and Dudhia*, 2001]. The OSU-LSM is a sophisticated Soil-Vegetation-Atmosphere Transfer model with four soil layers with a thickness of 10, 30, 60, and 100 cm, respectively. It calculates the soil temperature and moisture stratification and determines, in coordination with the planetary boundary layer (PBL) parameterization, the heat and moisture fluxes at the interface between atmosphere and soil. For vegetated surfaces, evapotranspiration and interception and reevaporation is taken into account.

[16] When the *Reisner Mixed-Phase* scheme [*Reisner et al.*, 1998] is used as an explicit moisture scheme in MM5, the model atmosphere is treated as composed of gas components dry air and water vapor and liquid and solid water particles. The particles are further partitioned in nonprecipitating fractions with negligible fall speed relative to the air (cloud particles) and fractions with uniform, only concentration-dependent fall speeds (precipitating particles). Water vapor and water particles are considered as continuously distributed in dry air so that time- and space-dependent three-dimensional mixing ratios (kg kg^{-1}) can be defined and used as prognostic variables:

[17] q_v: mixing ratio of water vapor (gas phase),

[18] q_c: mixing ratio of nonprecipitating liquid water substance (cloud droplets),

[19] q_i: mixing ratio of nonprecipitating solid water substance (cloud ice particles),

[20] q_r: mixing ratio of precipitating liquid water substance (rain droplets),

[21] q_s: mixing ratio of precipitating solid water substance (snow flakes and other solid forms).

2.2. Basic Model Equations for Humidity

[22] For the elaboration of the moisture tagging extensions in MM5, it is helpful to review the original transport equations for the water components. With q_k indicating the various mixing ratios q_v, q_c, q_i, q_r, q_s, the equations in flux form read as

$$\frac{\partial}{\partial t}(\rho_d q_k) = -\,\mathrm{div}(\rho_d q_k \mathbf{v}) - \mathrm{div}\mathbf{j}_{\mathrm{sub},k} - \mathrm{div}\mathbf{j}_{\mathrm{prc},k} + \rho_d C_k \tag{1}$$

or in advection form as

$$\frac{\partial}{\partial t} q_k = -\mathbf{v}\ \mathrm{grad} q_k - \frac{1}{\rho_d}\mathrm{div}\mathbf{j}_{\mathrm{sub},k} - \frac{1}{\rho_d}\mathrm{div}\mathbf{j}_{\mathrm{prc},k} + C_k \tag{2}$$

where ρ_d and $\mathbf{v}$ are the dry air density (kg m^{-3}) and the velocity (m s^{-1}) of dry air, respectively, while $\mathbf{j}_{\mathrm{sub},k}$ and $\mathbf{j}_{\mathrm{prc},k}$ are the flux densities (kg m^{-2} s^{-1}) of subgrid-scale transport and transport relative to the dry air by precipitating particles, respectively. C_k denotes the mass specific source rates (kg kg^{-1} s^{-1}) due to various transitions ("phase changes") between the moisture components. Evapotranspiration and precipitation fluxes are implicitly incorporated in equations (1) and (2). They are related to the boundary values of the flux densities $\mathbf{j}_{\mathrm{sub},k}$ and $\mathbf{j}_{\mathrm{prc},k}$ at the Earth's surface.

[23] The flux form (1) and the advection form (2) are physically equivalent. Often, the form (1) is the starting point for budget calculations. Integration of equation (1) over a specified constant volume ΔV with the boundary surface Ω gives

$$\frac{d}{dt}\int_{\Delta V} \rho_d q_k d\tau = -\int_{\Omega} (\rho_d q_k \mathbf{v} + \mathbf{j}_{\mathrm{sub},k} + \mathbf{j}_{\mathrm{prc},k})\ \mathbf{n}\ d\omega + \int_{\Delta V} \rho_d C_k\ d\tau \tag{3}$$

Equation (3) describes the mass change of moisture components in volume ΔV due to fluxes across the boundaries Ω with the normal unit vector $\mathbf{n}$ and phase transitions in the interior of ΔV. This equation is further applied in the results section.

[24] It is noted that in MM5, the advection equation (2) is chosen and written as

$$\begin{aligned}\frac{\partial}{\partial t}(p^* q_k) = &-m^2\left(\frac{\partial(p^* q_k m^{-1} u)}{\partial x} + \frac{\partial(p^* q_k m^{-1} v)}{\partial y}\right) - \frac{\partial(p^* q_k \dot{\sigma})}{\partial \sigma} \\ &+ q_k m^2\left(\frac{\partial(p^* m^{-1} u)}{\partial x} + \frac{\partial(p^* m^{-1} v)}{\partial y}\right) + q_k \frac{\partial(p^* \dot{\sigma})}{\partial \sigma} \\ &+ \mathrm{SUB}(q_k) + \mathrm{PRC}(q_k) + p^* C_k\end{aligned} \tag{4}$$

The moisture ratios q_k are here coupled with p^* (Pa). p^* denotes the time invariant difference of the reference pressures at the surface and model top. The two horizontal

Table 1. Phase Transition Processes in Explicit Moisture Scheme

Water vapor q_v	⇒ Cloud Water q_c	Cloud Condensation
	⇒ Cloud Ice q_i	Initiation to Cloud Ice
	⇒ Cloud Ice q_i	Deposition to Cloud Ice
	⇒ Rain Water q_r	Condensation to Rain
	⇒ Snow q_s	Deposition to Snow
Cloud water q_c	⇒ Water Vapor q_v	Evaporation of Cloud Water
	⇒ Rain Water q_r	Autoconversion to Rain
	⇒ Rain Water q_r	Collection of Cloud Water by Rain
	⇒ Snow q_s	Collection of Cloud Water by Snow
Cloud ice q_i	⇒ Water Vapor q_v	Sublimation of Cloud Ice
	⇒ Snow q_s	Autoconversion to Snow
	⇒ Snow q_s	Accretion of Snow by Cloud Ice
Rain water q_r	⇒ Water Vapor q_v	Evaporation of Rain
Snow q_s	⇒ Water Vapor q_v	Sublimation of Snow
	⇒ Water Vapor q_v	Evaporation of Melting Snow
	⇒ Rain Water q_r	Melting of Snow

coordinates in the chosen map projection are denoted by x (m) and y (m), the velocities in the corresponding directions by u (m s^{-1}) and v (m s^{-1}). The dimensionless variable σ is the terrain-following generalized vertical coordinate, with $\dot{\sigma}$ (s^{-1}) as its time derivative. The parameter m is the direction-independent map-scale factor arising from the map projection. As generally in all MM5 model equations, the advection in the moisture equation (4) is formulated in a pseudo flux form (first and second term on the right side) together with associated compensating divergence terms (third and fourth term). In analogy with equation (2), the other terms of equation (4) represent the subgrid-scale transport due to turbulence and diffusion SUB(q_k) (Pa kg kg^{-1} s^{-1}) especially in the planetary boundary layer, vertical downward transport by precipitation PRC(q_k) (Pa kg kg^{-1} s^{-1}), and water component transitions $p^* C_k$ (kg kg^{-1} s^{-1}). For the numerical solution of equation (4), second-order centered differences with a leapfrog time integration scheme are used. To avoid a splitting of the solution that is often associated with this three-time-level scheme, a time filter (Asselin filter) is applied after every time step.

[25] The "phase change" rates C_k of the five water components are combinations of single rates $C_{k,\alpha}$, where α indicates the various transition processes. Altogether, 16 different processes are considered and calculated by the explicit moisture scheme (Table 1). The scheme is for the first time activated as soon as saturation is reached in a grid cell. The fall speed of precipitating particles and the resulting vertical redistribution term PRC(q_k) for rain and snow components are also calculated.

[26] The vertical transport of water vapor from lower layers of the PBL to higher layers is essential for the fate of the tagged water substances. A significant part of the transport is associated with deep cumulus convection that can occur at scales which cannot be resolved by most atmospheric models. The collective effects of such subgrid-scale processes can be described only in terms of the large-scale model resolved environmental variables (Cumulus parameterization). At present, there are several schemes available based on different assumptions and formulations. A review of the cumulus parameterization problem is given for example by *Arakawa* [2004].

[27] In many cases the choice of the parameterization scheme strongly influences the results of global and regional model simulations. For West Africa, *Tchotchou and Kamga* [2010] investigated the sensitivity of a regional climate model to four different cumulus parameterization schemes. The results show that the West African monsoon precipitation is very sensitive to the choice of scheme. A similar result was confirmed by *Jung and Kunstmann* [2007] who performed regional climate simulations with different parameterizations for the Volta Region in West Africa.

[28] With regard to moisture tagging modeling, a consistent treatment by a cumulus parameterization scheme is difficult to achieve. Therefore, as reflected in the model equation (4), we do not apply any subgrid-scale cumulus parameterization. Instead, we use model resolutions generally assumed to be fine enough to capture at least those convection systems by grid-scale resolved dynamic model processes that are relevant for this study. We thus calculate the moisture transitions by an explicit scheme only.

2.3. ET-Tagging Algorithm

[29] For the moisture tagging option, new model variables representing the tagged water substances are defined. Corresponding to the five mixing ratios q_v, q_c, q_i, q_r, and q_s of the original moisture components, new mixing ratios $q_{v,\mathrm{tag}}$, $q_{c,\mathrm{tag}}$, $q_{i,\mathrm{tag}}$, $q_{r,\mathrm{tag}}$, and $q_{s,\mathrm{tag}}$ of the tagged moisture components are added. The original moisture variables remain unchanged. They now represent the sum of tagged and untagged moisture quantities.

[30] Accordingly, new model equations for the tagged moisture components are formulated and implemented accordingly in the RCM. With $q_{k,\mathrm{tag}}$ indicating $q_{v,\mathrm{tag}}$, $q_{c,\mathrm{tag}}$, $q_{i,\mathrm{tag}}$, $q_{r,\mathrm{tag}}$, and $q_{s,\mathrm{tag}}$, the equations read as

$$\begin{aligned}\frac{\partial}{\partial t}(p^* q_{k,\mathrm{tag}}) = &-m^2\left(\frac{\partial(p^* q_{k,\mathrm{tag}} m^{-1} u)}{\partial x} + \frac{\partial(p^* q_{k,\mathrm{tag}} m^{-1} v)}{\partial y}\right) \\ &- \frac{\partial(p^* q_{k,\mathrm{tag}}\dot{\sigma})}{\partial \sigma} + q_{k,\mathrm{tag}}\left(m^2\left(\frac{\partial(p^* m^{-1} u)}{\partial x}\right.\right. \\ &\left.\left. + \frac{\partial(p^* m^{-1} v)}{\partial y}\right) + \frac{\partial(p^*\dot{\sigma})}{\partial \sigma}\right) \\ &+ \mathrm{SUB}(q_{k,\mathrm{tag}}) + \mathrm{PRC}(q_{k,\mathrm{tag}}) + p^* C_{k,\mathrm{tag}} \qquad (5)\end{aligned}$$

Equation (5) describes the same processes as equation (4) for the original moisture variables. In the transport schemes, identical advection velocities and turbulence intensities are applied. Also, the fall velocity is the same for tagged and untagged precipitating particles, only dependent on the total content of rain and snow substances, respectively. Analogously to the transition rates C_k between the total water components, the transition rates $C_{k,\mathrm{tag}}$ between the tagged water components are combinations of single rates $C_{k,\alpha,tag}$ for the various transition processes. These rates $C_{k,\alpha,\mathrm{tag}}$ are proportional to the transition rates $C_{k,\alpha}$ between the original total water components and in proportion to the ratio of the relevant tagged and the corresponding total parts. As an example, for the process collection of cloud water by snow the transition rates, $C_{s,\mathrm{collection}}$ and $C_{s,\mathrm{collection,tag}}$ are related by $C_{s,\mathrm{collection,tag}} = C_{s,\mathrm{collection}}\, q_{c,\mathrm{tag}}\, q_c^{-1}$.

[31] The formation of tagged moisture starts with the evaporation process at the land surface. The moisture then enters the first (lowest) atmospheric model layer and thereby the PBL. In equation (5), this is accounted for by the term SUB($q_{k,\mathrm{tag}}$). All the water substance evaporating from a user-specified tagging source area is then tagged and tracked through all atmospheric transport processes (advection terms and SUB($q_{k,\mathrm{tag}}$)). The tagged water vapor is subject to phase

transition processes ($C_{k,\mathrm{tag}}$). It can move through the atmosphere and partly fall out as precipitation (PRC($q_{k,\mathrm{tag}}$)).

[32] A tagged water substance can leave the atmosphere through outflow at the lateral model domain boundaries. Returning tagged water from outside of the model domain is not taken into account. This is expressed as a lateral boundary condition "no flux at inflow and zero flux gradient at outflow."

[33] When the equations describing the phase transition and precipitation formation processes in the explicit moisture scheme are solved, numerical problems can arise as the numerical solution yields negative or zero values instead of small positive definite moisture values. One reason for negative values of the condensed moisture variables may be the advection scheme, which is not strictly mass conserving and not positive definite. Therefore, the equations are only applied and solved if the values of the involved variables exceed specified threshold values and resulting small negative values are set to zero. In the added tagged moisture equations, additional criteria for the ratios of tagged to total moisture quantities have to be defined. They must be carefully chosen so that the handling of the additional equations are more or less consistent with the handling of the original (i.e., total moisture) equations.

[34] During phase transitions, the sum $q_{\mathrm{tot,tag}}$ of all tagged water variables remains constant. The only source for $q_{\mathrm{tot,tag}}$ is evaporation in the tagging area; the only sinks are precipitation and outflow from the model domain. Precipitating tagged water no longer remains tagged as there is no subsurface tagged moisture in our approach. Tagged water precipitating outside the tagging area is fully lost, while in the tagging area, reevaporated formerly tagged precipitation water can return as a newly tagged quantity to the system.

3. The Experimental Setup

[35] To demonstrate the analysis potential of our explicit moisture tagging approach and to point out the important influence of vertical transport, we have applied the extended model to West Africa and performed relatively highly resolved simulations for the 2 month period of July and August of 1998. With the exception of the coastal areas at the Gulf of Guinea, the maximum precipitation is generally received in August [*Xue et al.*, 2010], i.e., the second month of simulation. The model is initialized and driven by global reanalysis data from the NCEP/NCAR Reanalysis Project [*Kalnay et al.*, 1996], which is available every 6 h. These global data provide the initial and boundary values for the atmosphere, initial values for soil temperature and humidity, and sea surface temperatures (SSTs).

[36] We applied the regional model with the Mercator projection option and used a model domain extending from 2.73°N to 19.05°N and from 9.34°W to 7.34°E, covering the Volta Basin and a sufficiently wide border zone (see Figures 1 and 2). Geographical data describing terrain elevation, land use (24 category U.S. Geological Survey (USGS) data), and soil characteristics (17 category FAO data) were taken from NCAR data sets.

[37] For the simulation, referred to as *Sim09* in the following, we have chosen a horizontal grid spacing of 9 km, assuming that the grid is fine enough to capture the most relevant convective systems. This resulted in a horizontal

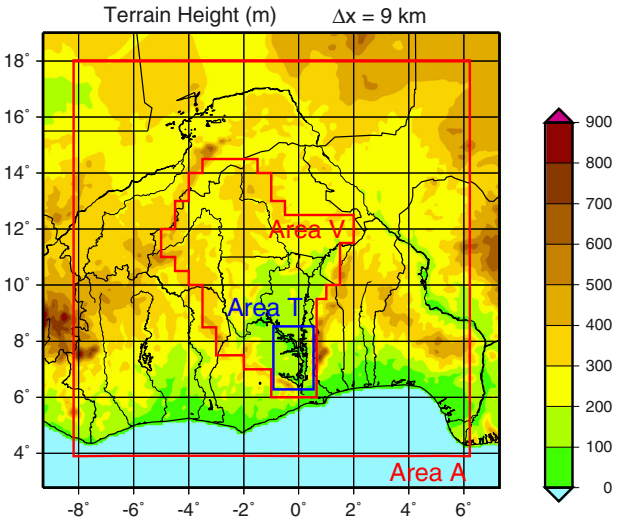

Figure 2. Model domain with terrain height (m) as used in *Sim09*. Also marked are the tagging area T, the analysis area V (Volta Basin), and the analysis area A.

model configuration with $206 \times 206 = 42,436$ grid cells. For the vertical structure, we used 33 model layers from the Earth's surface up to the 50 hPa level, where a rigid upper boundary is assumed. The basic time step was 25 s.

[38] The SSTs provided by NCEP are only applied to the ocean surface. Over the continent, we calculated surface temperature of the model-resolved lakes (Lake Volta and some smaller lakes) based on data published by the *International Lake Environment Committee* [2012]. For July, we use 29.0°C, for August 28.0°C.

[39] As the "tagging water source area," we defined a small area (about 40,800 km^2) around Lake Volta, hereafter referred to as area T (see Figure 2). Nearly 12% of the grid cells in this area represent water bodies. The rest of the grid cells belong predominantly to the USGS Category *Savanna* or, in particular in the southern and eastern parts, to the category *Cropland/Wood Mosaic*. In addition, two analysis areas, area V and area A, are defined and shown in Figure 2. Area V represents approximately the Volta Basin. Area A encompasses the whole model domain, with the exception of a 14 grid cells wide border zone and is used to calculate area average values approximately representing model domain means thereby avoiding possible boundary effects.

4. Results and Discussion

[40] The simulation *Sim09* covers the period from 00:00 UTC 1 July to 00:00 UTC 1 September 1998. Initially, the tagged moisture ratios are set to zero. Then, all the water substance evaporating from the surface in area T is tagged and tracked until it leaves the atmospheric part of the model domain either through precipitation on the Earth's surface or through outflow at the lateral domain boundaries. After several days, the model adopts an adjusted regional-scale meteorological state and a quasi balanced distribution of the tagged moisture. Therefore, we consider the first simulated month as a "spin up" time period and present monthly means and budget calculations for the second simulated month, August 1998.

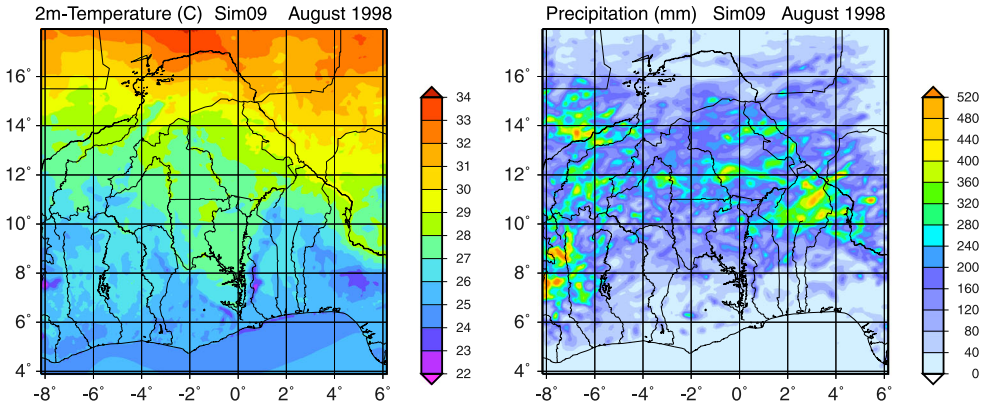

Figure 3. Monthly mean of 2 m temperature in °C (left) and monthly precipitation sum in mm (right) as simulated in *Sim09* for August 1998.

4.1. Simulated General Atmospheric Conditions

[41] Figure 3 shows the monthly mean of the 2 m temperature and the monthly precipitation sum as calculated in *Sim09* for August 1998. The overall simulated temperature increases from the Guinean Coast in the south to the sub-Saharan region in the north appear to resemble the known observed climate reasonably well. With regard to precipitation, the simulation reproduces the basic climatic characteristics of the rainy season for the month of August. The maxima found in the southwest area of the model domain (around 8°W and 8°N) and in a broad latitudinal band between 9°N and 15°N are in general accordance with observed values, e.g., with data reported in the work of *Nicholson et al.* [2003, see their Figure 10].

[42] However, it cannot be expected that the regional model will simulate every single observed precipitation event correctly and reproduce the observed precipitation pattern down to the local station scale exactly. Since the boundary forcing contains only the preconditions for the formation of convective elements, the regional model can develop circulations more or less differently from that of the driving NCEP analysis data and on scales not resolved by the reanalysis model. Nearly randomly distributed fine-scale convective structures and precipitation patterns can be generated by the model that makes it difficult to directly compare with reality. The direct comparison of modeled and observed precipitation values in the scatterplot of Figure 4 shows this limitation. When looking closer to points which show larger deviations between model and observation, however, it is seen from Figure 5 that in many cases in immediate proximity, the model is approaching closer to the observed station values. The results are of comparable performance as, e.g., in *Wagner et al.* [2009]. In general, we conclude that the RCM reasonably reproduces observed precipitation patterns.

[43] One of the characteristic features in West Africa is the monsoon circulation. During the rainy season in the summer months, southwesterly winds dominate near the surface and easterly winds at higher levels [*Cook*, 1999]. Figure 6 shows the wind field as simulated by the RCM in *Sim09* for August 1998. Here the monthly means of the wind field in the lowest model layer (left) and in the seventeenth layer (a middle model layer with a reference pressure of about 660 hPa, roughly around 3400 m height) (right) are displayed.

[44] Figure 6 shows (in the monthly mean) a quite homogeneous wind field with a moderate southwest to northeast movement near the surface and stronger, rather homogeneous easterly winds in the upper layer. These features of the simulated wind field are in general accordance to reanalysis data as shown, e.g., in the works of *Moufouma-Okia and Rowell* [2010] and *Patricola and Cook* [2010]. As a consequence of the changing wind direction and wind speed with height, the atmospheric transport is essentially three-dimensional (see also Figure 8). This is of crucial relevance for the distributions of the tagged moisture quantities, as is shown in the next sections.

4.2. Evolution of the Tagged Moisture Field

[45] To illustrate the evolution of the tagged moisture, we consider the first simulated days in July. Figure 7 shows the spatial distributions of the total tagged moisture content $q_{\mathrm{tot,tag}}$ near the surface at six different times. The figures indicate the variations due to day-night differences of evaporation and show the transport and spreading of the moisture pattern.

[46] At the start, there is no tagged moisture in the model domain. After that, moisture evaporating from the tagging

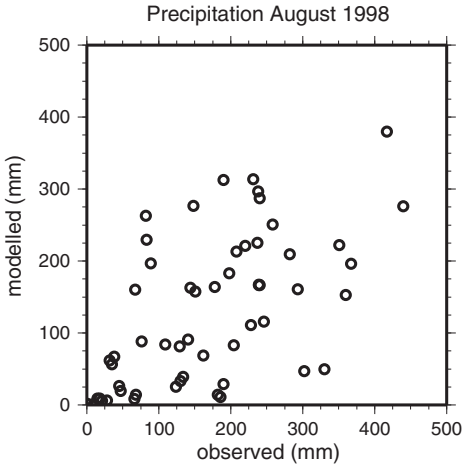

Figure 4. Scatterplot of monthly precipitation sum (mm) as simulated in *Sim09* and of observed station data provided by the *National Climatic Data Center* [2012] for August 1998.

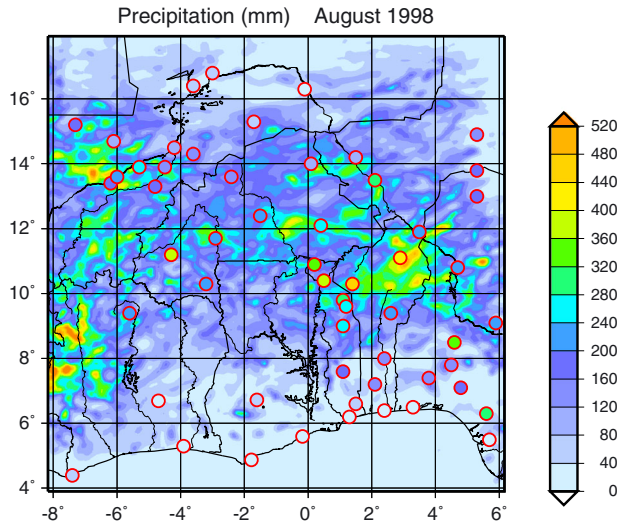

Figure 5. Comparison of monthly precipitation sum (mm) as simulated in *Sim09* and of observed station data (depicted as circles) provided by the *National Climatic Data Center* [2012] for August 1998.

source area T around Lake Volta enters the atmosphere as tagged water vapor. The further evolution of the tagged moisture is first governed by the horizontal wind field, which is quite similar to the monthly mean wind field for August, displayed in Figure 6. Of course, exceptions with distinctly different wind patterns may be found locally, especially near areas with strong convective events.

[47] A closer look at the wind situation on the second day of July in the region near the tagging source area T is given in Figure 8, showing the vertical profiles of the west-east and south-north wind components u and v, averaged over area T. In a layer between the surface and a level of around 850 hPa, the wind direction is west to southwest. This is reflected in the evolution of the tagged water field shown in Figure 7. The evaporated water from the Lake Volta region thus travels to the east and northeast. Since the tagged water spreads over the whole planetary boundary layer, the concentration in the lowest model layer gradually decreases with distance from the source area T.

[48] In the upper layers above about 850 hPa, mainly easterly winds with a maximum speed at about 700 hPa prevail (Figure 8). The moisture evaporating from the source area T can usually reach these upper levels to a significant extent only if air from the boundary layer is lifted. The most effective mechanism is lifting by extended cumulus or cumulonimbus convection systems.

[49] To get information about the convective state in the model domain, the column-integrated condensed moisture W_{cond} (kg m^{-2}) is used as an indicator for intense cloud and precipitation formation. This and the related quantities for tagged condensed moisture $W_{\mathrm{cond,tag}}$ (kg m^{-2}) and for tagged total moisture $W_{\mathrm{tot,tag}}$ (kg m^{-2}) are defined as

$$W_{\mathrm{cond}} = \int_{z_{\mathrm{sfc}}}^{z_{\mathrm{top}}} \rho_d q_{\mathrm{cond}}\, dz \tag{6}$$

$$W_{\mathrm{cond,tag}} = \int_{z_{\mathrm{sfc}}}^{z_{\mathrm{top}}} \rho_d q_{\mathrm{cond,tag}}\, dz \tag{7}$$

$$W_{\mathrm{tot,tag}} = \int_{z_{\mathrm{sfc}}}^{z_{\mathrm{top}}} \rho_d q_{\mathrm{tot,tag}}\, dz \tag{8}$$

with q_{cond} (kg kg^{-1}) denoting the mixing ratio of condensed moisture content (sum of cloud water, cloud ice, rain, and snow content), $q_{\mathrm{cond,tag}}$ (kg kg^{-1}) the mixing ratio of tagged condensed moisture content, $q_{\mathrm{tot,tag}}$ (kg kg^{-1}) the mixing ratio of tagged total moisture content, and z_{sfc} and z_{top} the heights (m) of the surface and top level of the model domain, respectively.

[50] The spatial distribution of the integrated quantities W_{cond} and $W_{\mathrm{cond,tag}}$ is depicted in Figure 9. Also shown is the spatial distribution of the total tagged moisture ratio $q_{\mathrm{tot,tag}}$ in the seventeenth model layer (about 3400 m height). The fields are each presented for the 2 times 18:00 UTC 2 July 1998 and 00:00 UTC 3 July 1998, allowing an assessment of the horizontal movement and tendency strength of the convective systems between these times.

[51] Figure 9 (upper row) shows a large cloud and precipitation system moving from east to west in the northern part of the model domain with extensions to the northern borders of Ghana, Togo, and Benin. Further intensive single

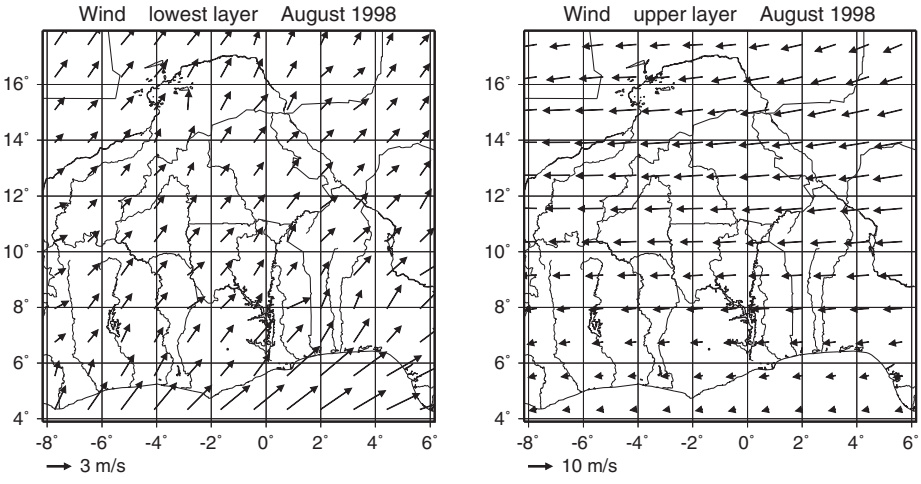

Figure 6. Monthly mean of horizontal wind in the lowest model layer (left) and in the 17th model layer (around 3400m, right) as simulated in *Sim09* for August 1998.

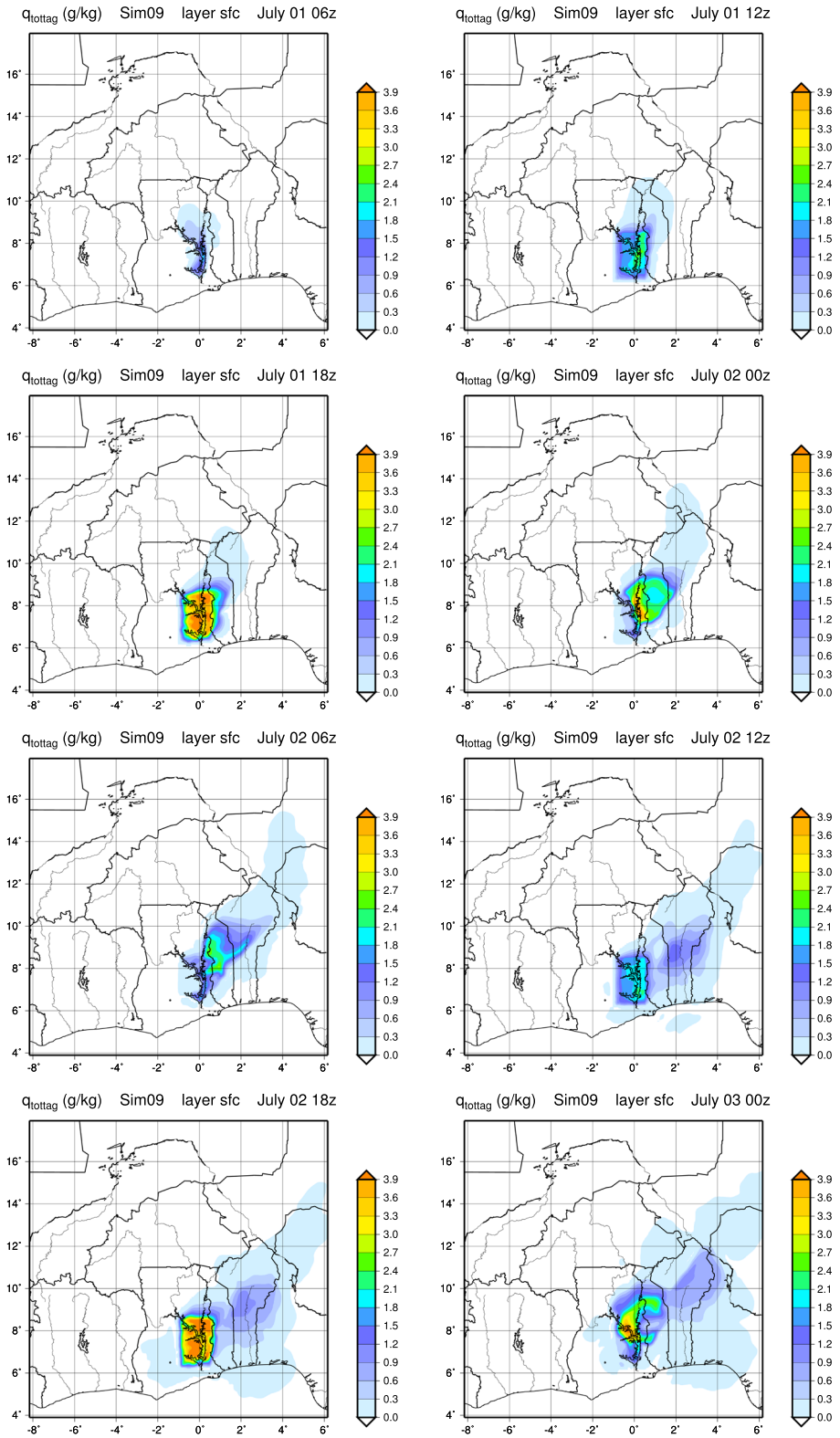

Figure 7. Total tagged moisture $q_{\mathrm{tot,tag}}$ (g kg^{-1}) in the lowest model layer at different times during the first 2 days (06:00 UTC 1 July to 00:00 UTC 3 July 1998) of simulation *Sim09*.

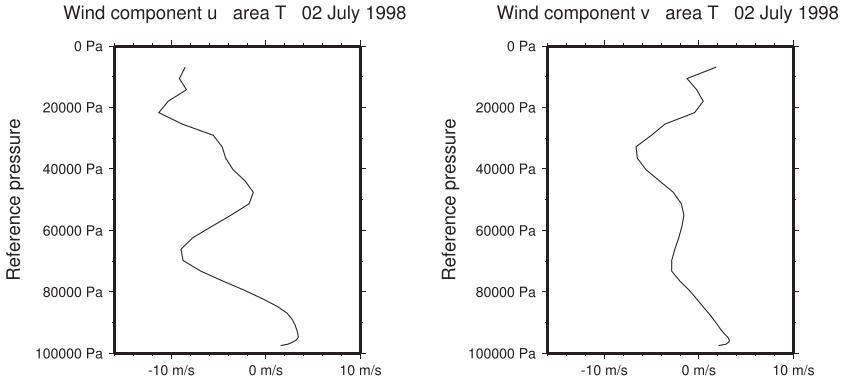

Figure 8. Vertical profile of west-east wind component u (m s^{-1}) and south-north component v (m s^{-1}) as simulated in *Sim09*, averaged over area T, 2 July 1998.

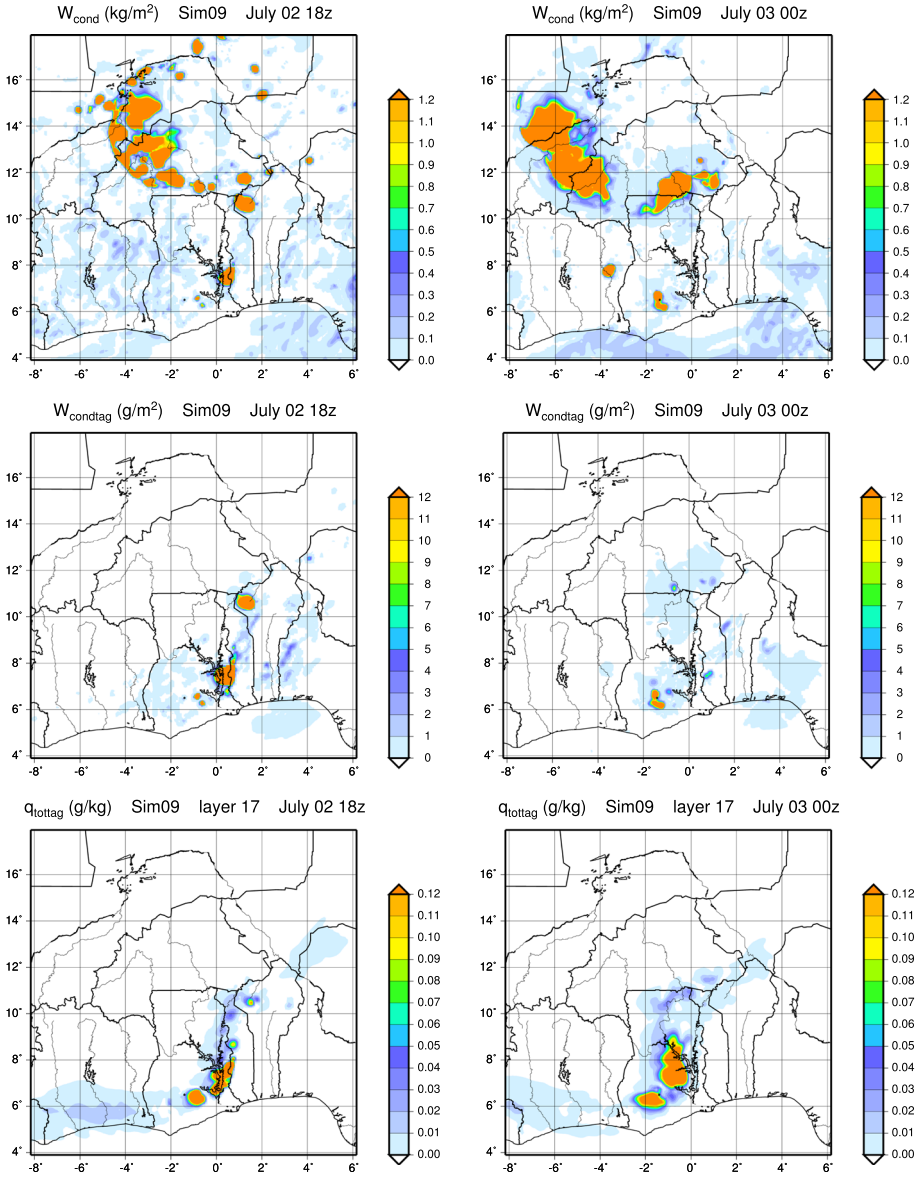

Figure 9. Distributions of column-integrated condensed moisture W_{cond} (kg m^{-2}) (upper row), column-integrated tagged condensed moisture $W_{\mathrm{cond,tag}}$ (g m^{-2}) (middle row), and mixing ratio of tagged total moisture content $q_{\mathrm{tot,tag}}$ (g kg^{-1}) in the seventeenth model layer around 3400 m (lower row) as simulated in *Sim09*, each for 18:00 UTC 2 July 1998 (left) and for 00:00 UTC 3 July 1998 (right).

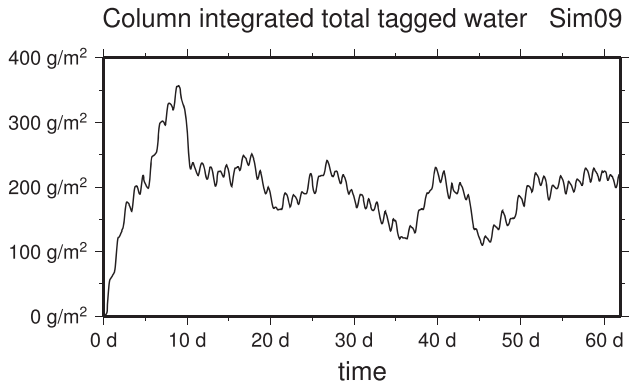

Figure 10. Time series of 1 July to 31 August 1998 of column-integrated total tagged moisture $W_{tot,tag}$ (g m^{-2}) as simulated in *Sim09* averaged over the analysis area A.

convection systems are found at 18:00 UTC 2 July immediately near Lake Volta, one bigger system to the east, and two smaller ones southwest of the Lake. These systems also move to the west in accordance with the prevailing wind in the upper atmospheric layers over the tagging area T as shown in Figure 8.

[52] If tagged evaporated water in the boundary layer is part of these convective systems, the tagged moisture can condensate and be lifted to upper levels. It then contributes to the local precipitation or is transported with the prevailing winds to westerly regions and eventually precipitates downstream. As indicated in Figure 9 (middle row) in our specific evaluation period, this takes place in the abovementioned convective systems in the northwest corner of Benin and around Lake Volta.

[53] The westward traveling systems contain a significant amount of tagged water. The typical resulting spatial distribution of the total tagged moisture content $q_{tot,tag}$ in upper atmospheric layers is shown for the seventeenth model layer in Figure 9 (lower row). At 00:00 UTC 3 August, the highest values are found west of Lake Volta and at the northern border of Ghana. In the boundary layer of the source area, there is no direct horizontal (westward) wind transportation to these locations. Therefore, the higher values of tagged moisture pattern in the northern part of Ghana can only be explained when the fully three-dimensional wind field is accounted for: near-surface eastward transport of evaporated water from the Lake Volta region to the northeast near the northern border of Benin, lifting largely by convection, and then transport in upper layers to the west.

[54] Figure 10 shows a time series of the column-integrated total tagged moisture $W_{tot,tag}$ averaged over the analysis area A for the whole simulation period during July and August. During the first days, the tagged moisture increases nearly monotonically in the model atmosphere until the loss due to precipitation or outflow at the lateral model boundaries approximately balances the gain due to evaporation in the source area. On about daily time scales, there are intense fluctuations likely reflecting the interplay of the day-night cycle of evaporation and precipitation. At periods of about 5 days or more, variations are exhibited that are comparable with the time that extended precipitation systems need to travel through the model domain from east to west.

4.3. Tagged Moisture Budgets

[55] As shown in Figure 10, the vertically integrated total tagged moisture $W_{tot,tag}$ of the model atmosphere exhibits no overall systematic trend in the second month of the simulation period. Figure 11 shows the spatial distribution averaged over August. As expected, the maximum of tagged moisture can be found in the source area T with values of about 2000 g m^{-2}. The tagged moisture, averaged over the whole area T, amounts to 1258 g m^{-2} which represents only 2.5% of the total moisture. Outside the source area, the moisture content decreases generally with distance. As the largest part of both the atmospheric total and tagged moisture resides in the planetary boundary layer, the distribution of $W_{tot,tag}$ is mainly determined by the conditions in the lower atmosphere with transport from southwest to northeast (cf. Figure 6). This also explains the sharp moisture gradient near the western and southern borders of the source area T and the formation of a tagged moisture plume in the northeast.

[56] Figure 11 also shows the spatial distribution of the column-integrated condensed tagged moisture $W_{cond,tag}$. Since the condensed moisture is mainly a result of lifting processes by convective systems traveling from east to west, the resulting distribution is comparatively complex and clearly different from the total moisture distribution. Higher values of tagged condensed moisture appear above the before mentioned plume of $W_{tot,tag}$ with maxima directly east of Lake Volta and in the northern part of Benin. Two further patterns with higher values are found over Burkina Faso. They exhibit a band-like structure, suggesting that this structure was formed during the simulation by only a few large cloud and precipitating systems which travel from east to west, thereby incorporating a significant amount of tagged moisture.

[57] The pattern of the monthly sum of tagged precipitation (Figure 12, left) is directly linked to the mean tagged condensed moisture distribution. Most of the simulated precipitation of tagged water appears up to several hundred kilometers northeastward of the source area. The highest values are found next to Lake Volta. The band-like structures found in the distribution of $W_{cond,tag}$ over Burkina Faso (Figure 11, right) also appear in the precipitation distribution (Figure 12). Generally, the pattern of condensed moisture and precipitation are very similar.

[58] To quantitatively evaluate the relevance of the recycled part of precipitation, we analyze additionally the local precipitation ratio α of tagged precipitation density j_{tag} (kg m^{-2}) to total precipitation density j (kg m^{-2}).

$$\alpha(x,y) = j_{tag}(x,y)\ j^{-1}(x,y) \tag{9}$$

Figure 12 (right) shows the spatial distribution of the monthly mean of α for August 1998. Near Lake Volta, up to 6% of the total precipitation are of local origin. Some hundred kilometers away predominantly less than 1% of the precipitated water originated from the tagging source area. Higher values of more than 1% are only found in parts of Burkina Faso and generally at some locations in the eastern part of the model domain. The value for the whole analysis area A averages to less than 1%.

[59] If the ratio of the area-integrated tagged precipitation R_{tag} (kg) and total precipitation R (kg) is considered, a dimensionless parameter r_{reg} is obtained, which is in

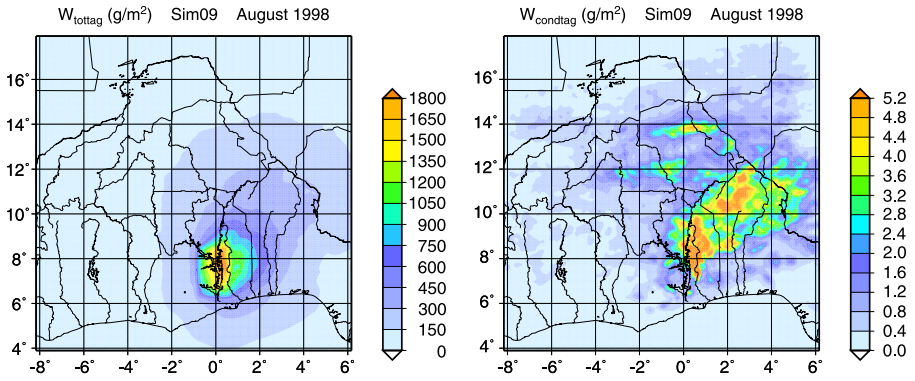

Figure 11. Column-integrated total tagged moisture $W_{\mathrm{tot,tag}}$ (g m^{-2}) (left) and column-integrated condensed tagged moisture $W_{\mathrm{cond,tag}}$ (g m^{-2}) (right), averaged over August 1998 as simulated in *Sim09*.

the literature often termed as regional moisture recycling ratio for a specified moisture source area [e.g., *van der Ent et al.*, 2010].

$$r_{\mathrm{reg}} = R_{\mathrm{tag}}\ R^{-1} \tag{10}$$

Principally, this regional recycling ratio r_{reg} ranges from zero, when the size of the considered area is small, to near unity, when the area of investigation becomes very large. In our study, the recycling ratio for the Lake Volta Region (area T) amounts to around 3% with our regional ET-tagging approach.

[60] A further central question to be addressed with the presented ET-tagging approach is "where does the water evaporating in the source region (area T) finally end up?" To investigate this, we consider the total tagged water mass $Q_{A,\mathrm{tag}}$ (kg) in the model domain partition V_A above the analysis area A:

$$Q_{A,\mathrm{tag}} = \int_{V_A} \rho_d q_{\mathrm{tot,tag}} d\tau \tag{11}$$

Applying the general budget equation (3) for the tagged and the total moisture sum of all components in the model partition V_A, the phase transition terms vanish. Due to model boundary conditions, the flux terms reduce to evaporation and precipitation fluxes at the surface and atmospheric fluxes at the lateral boundaries. Integration over a time period Δt then yields the following conservation equation:

$$\Delta Q_{A,\mathrm{tag}} = E_{A,\mathrm{tag}} - P_{A,\mathrm{tag}} - F_{A,\mathrm{tag}} \tag{12}$$

Equation (12) describes the change $\Delta Q_{A,\mathrm{tag}}$ during the time period Δt. This is a result of gain by evaporation $E_{A,\mathrm{tag}}$ (kg) from area A, loss by precipitation $P_{A,\mathrm{tag}}$ (kg) in area A, and gain or loss by net outflow $F_{A,\mathrm{tag}}$ (kg) of tagged moisture across the lateral boundaries of the domain partition V_A. As all tagged evaporated water in area A originates from the subarea T, the evaporation quantity $E_{A,\mathrm{tag}}$ is identical to the evaporation $E_{T,\mathrm{tag}}$ (kg) from area T.

[61] Changes in the moisture contents $\Delta Q_{A,\mathrm{tag}}$ and the evaporation $E_{A,\mathrm{tag}}$ as well as precipitation $P_{A,\mathrm{tag}}$ can be derived directly from the model output. The net lateral outflow $F_{A,\mathrm{tag}}$, however, can only be determined indirectly as residual according to equation (12). Rearranging equation (12), replacing $E_{A,\mathrm{tag}}$ by $E_{T,\mathrm{tag}}$ and splitting $P_{A,\mathrm{tag}}$ in $P_{T,\mathrm{tag}} + P_{V^*,\mathrm{tag}} + P_{A^*,\mathrm{tag}}$ yield

$$E_{T,\mathrm{tag}} = P_{T,\mathrm{tag}} + P_{V^*,\mathrm{tag}} + P_{A^*,\mathrm{tag}} + F_{A,\mathrm{tag}} + \Delta Q_{A,\mathrm{tag}} \tag{13}$$

with $P_{V^*,\mathrm{tag}}$ as precipitation outside of area T but inside of area V and $P_{A^*,\mathrm{tag}}$ as precipitation outside of area V but inside of area A. The values of all tagging variables appearing in equation (13) and the values of tagged and total precipitation in area T, area V, and area A as calculated in the model simulation *Sim09* for the period August 1998 are listed in Table 2.

[62] Equation (13) describes the fate of the evaporated (tagged) moisture in the area A. In our simulation for August 1998, only 1.7% of the tagged evaporated water $E_{T,\mathrm{tag}}$ is

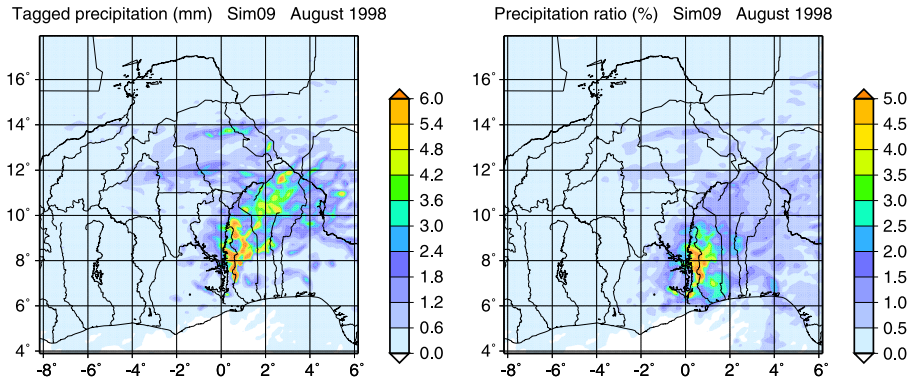

Figure 12. Monthly sum of tagged precipitation in mm (left) and monthly mean of precipitation ratio α (right) as simulated in *Sim09*.

Table 2. Terms of the Total Tagged Moisture Budgets According to Equation (13) and Tagged and Total Precipitation Sums for Area T, Area V, Area V* (the Area Outside of T but Inside of V), Area A, and Area A* (the Area Outside of V but Inside of A) as Calculated in *Sim09* for August 1998

		Precipitable Water (mm)	Water Mass (10^9 kg)	%
$E_{T,\mathrm{tag}}$	Tagged Evaporation Over T	90.1	3 676.4	100.0
$P_{T,\mathrm{tag}}$	Tagged Precipitation Over T	1.5	61.8	1.7
$P_{V^*,\mathrm{tag}}$	Tagged Precipitation Over V^*	0.9	359.1	9.8
$P_{A^*,\mathrm{tag}}$	Tagged Precipitation Over A^*	0.5	990.7	26.9
$F_{A,\mathrm{tag}}$	Net Tagged Outflow From V_A		2 203.3	59.9
$\Delta Q_{A,\mathrm{tag}}$	Change of Tagged Water in V_A	0.02	61.6	1.7
$P_{V,\mathrm{tag}}$	Tagged Precipitation Over V	1.0	420.8	
$P_{A,\mathrm{tag}}$	Tagged Precipitation Over A	0.6	1 411.5	
P_T	Total Precipitation Over T	54.0	2 204.3	
P_V	Total Precipitation Over V	153.5	64 404.7	
P_A	Total Precipitation Over A	115.8	297 097.2	

recycled as precipitation in the source area. Nearly all the rest is transported out of the source region. Farther 9.8% of $E_{T,\mathrm{tag}}$ precipitates in the rest of the Volta basin (subarea V*) and farther 26.9% in the surrounding subarea area A* of area A. Nearly 60% leaves the model domain partition V_A by transport over the outer lateral boundaries. When related to the total catchment area V and to the total area A, the tagged precipitation is 11.5% and 38.4%, respectively.

[63] Since nearly all the water evaporated in area T leaves this area, the contribution of the local evaporation to the precipitation in area T accounts, as previously mentioned for only around 3% of the total. The rest is imported from outside as untagged water. With respect to the larger Volta basin (area V), less than 1% of the precipitation has its origin in the tagging area T.

[64] The ratios of tagged and total precipitation as calculated in this simulation can be regarded as lower limits, since the model does not allow for inflow of tagged water substance from outside the model boundaries. Tagged moisture which leaves the model domain is lost and cannot return as a tagged quantity.

5. Summary and Conclusions

[65] A detailed evaporation tagging mechanism was implemented in the regional climate model MM5. The model was applied with high spatial and temporal resolution to the analysis of a 1 month period in the rainy season 1998 in the Volta Basin in tropical West Africa. The RCM reproduces the basic patterns of temperature and precipitation and is able to reasonably display the observed changing wind directions with height, mechanisms that impact and control the spatial distribution of moisture fields, followed by the formation of precipitation systems. Since the tagging mechanism is fully three-dimensional, it accounts for vertical movements and height-dependent horizontal transport.

[66] The study shows the evolution of the tagged moisture field and reveals details of the transport that cannot be seen in bulk-type approaches or in coarser resolved models. Moisture evaporated from Lake Volta is initially transported predominantly to the east and north, lifted by convective processes and then transported to west. In the model simulations, only a small part of the moisture is lifted before reaching the model boundaries. The results clearly indicate that the coupling between boundary layer and higher atmospheric levels through convective processes can be essential for the fate of tagged water substances. Local vertical transport of water vapor from lower layers of the PBL to higher layers with changed wind direction and increased horizontal wind speed largely determine the distribution of tagged water in remote areas far away from the source of evaporation.

[67] With a resolution of 9 km, the model simulates a more or less realistic precipitation distribution, mainly produced by large convective complexes. Our results are in general agreement with analyses that show that mesoscale convective systems account for most of the rain in the Sahel and about half of the rain in the Soudanian zone [*Lafore et al.*, 2011]. It is safe to assume that a higher grid resolution alters the intensity and structure of the large modeled convective systems and additionally generates new smaller-scale systems. How far this influences the distribution of tagged moisture and the resulting recycling parameters has to be answered by further studies. Likewise, a detailed analysis of the influence of the chosen parameterizations and numerical schemes on the tagging results is required in the future.

[68] In this study, a comparatively small area around Lake Volta was chosen as the source area for the tagged water substance. The regional recycling ratio for the source area calculated here accounts for just about 3%. This is considerably smaller than recycling ratios for larger basins obtained by alternative, mostly bulk-type approaches. Literature values, as reported by, e.g., *Mohamed et al.* [2005], vary between 24 and 50% for the Amazon Basin and between 10 and 47% for the Mississippi Basin. For the Nile Basin, which covers an area of over 3 million km^2 and thereby is more than 75 times larger than our source area around Lake Volta, *Mohamed et al.* [2005] calculated an annual mean of the recycling ratio of about 11%, i.e., around 4 times higher than the value derived in this study.

[69] In our case study, only less than 2% of the water evaporated from the Lake Volta region is locally recycled as precipitation while the rest is transported out of the source region. Nearly 60% of the tagged moisture leaves the model domain. We assume that in a larger model domain, tagged moisture in lower layers traveling to the eastern boundary gets a further chance to be lifted to higher levels and

then transported back by the easterly winds. In addition, a larger amount of tagged water in higher layers traveling to the western boundary can reach lower layers by mixing or by precipitation evaporation. Through the dominant monsoon winds, the tagged water is then transported back and hence does not leave the model domain. Both processes could account for a longer life cycle of the tagged moisture in a larger model domain, thereby yielding higher recycling values.

[70] In the future, our proposed regional high-resolution evaporation tagging approach is envisaged to be applied to further hydroclimatologically sensitive regions like, e.g., large-scale irrigation schemes in different climate zones worldwide. Our presented fully three-dimensional evaporation tagging approach might also be beneficial in high mountain regions that are able to significantly block and deflect raising humid air masses from evaporating wet areas.

[71] **Acknowledgments.** This work was initiated during the GLOWA-Volta project (http://www.glowa-volta.de) and continued in the WASCAL project (http://www.wascal.org). We thank Hans Peter Schmid (KIT/IMK-IFU) for his valuable comments and suggestions. The help of Richard Foreman (KIT/IMK-IFU) and Dominikus Heinzeller (KIT/IMK-IFU) for proofreading the manuscript is gratefully acknowledged.

References

Arakawa, A. (2004), The cumulus parameterization problem: Past, present, and future, *J. Clim.*, *17*, 2493–2525.

Bosilovich, M. G., and S. D. Schubert (2002), Water vapor tracers as diagnostics of the regional hydrologic cycle, *J. Hydrometeorol.*, *3*, 149–165.

Brubaker, K. L., D. Entekhabi, and P. S. Eagleson (1993), Estimation of continental precipitation recycling, *J. Clim.*, *6*, 1077–1089.

Burde, G. I., and A. Zangvil (2001), The estimation of regional precipitation recycling. Part I: Review of recycling models, *J. Clim.*, *14*, 2497–2508.

Chen, F., and J. Dudhia (2001), Coupling an advanced land surface-hydrology model with the Penn State/NCAR MM5 Modeling System. Part I: Model implementation and sensitivity, *Mon. Weather Rev.*, *129*, 569–585.

Cook, K. H. (1999), Generation of the African Easterly Jet and its role in determining West African precipitation, *J. Clim.*, *12*, 1165–1184.

Dirmeyer, P. A., and K. L. Brubaker (1999), Contrasting evaporative moisture sources during the drought of 1988 and the flood of 1993, *J. Geophys. Res.*, *104*(D16), 19,383–19,397.

Druyan, L. M., and T. M. Hall (1996), The sensitivity of African wave disturbances to remote forcing, *J. Appl. Meteorol.*, *35*, 1100–1110.

Druyan, L. M., M. Fulakeza, and P. Lonergan (2006), Mesoscale analyses of West African summer climate: Focus on wave disturbances, *Clim. Dyn.*, *27*, 459–481, doi:10.1007/s00382-006-0141-9.

Dudhia, J. (1993), A nonhydrostatic version of the Penn State/NCAR Mesoscale Model: Validation tests and simulation of an Atlantic cyclone and cold front, *Mon. Weather Rev.*, *121*, 1493–1513.

Eltahir, E. A. B., and R. L. Bras (1994), Precipitation recycling in the Amazon basin, *Q. J. R. Meteorol. Soc.*, *120*, 861–880.

Eltahir, E. A. B., and R. L. Bras (1996), Precipitation recycling, *Rev. Geophys.*, *34*, 367–378.

Gimeno, L., A. Stohl, R. M. Trigo, F. Dominguez, K. Yoshimura, L. Yu, A. Drumond, A. M. Durán-Quesada, and R. Nieto (2012), Oceanic and terrestrial sources of continental precipitation, *Rev. Geophys.*, *50*, RG4003, doi:10.1029/2012RG000389.

Goessling, H. F., and C. H. Reick (2011), What do moisture recycling estimates tell? Lessons from an extreme global land-cover change model experiment, *Hydrol. Earth Syst. Sci.*, *8*, 3217–3235, doi:10.5194/hess-15-3217-2011.

Grell, G. A., J. Dudhia, and D. R. Stauffer (1995), A description of the fifth-generation Penn State/NCAR Mesoscale Model (MM5), *Tech. Note NCAR/TN-398+STR*, 132 pp., Natl. Cent. for Atmos. Res., Boulder, Colo.

Hong, S.-Y., and H.-L. Pan (1996), Nonlocal boundary layer vertical diffusion in a medium-range forecast model, *Mon. Weather Rev.*, *124*, 2322–2339.

International Lake Environment Committee (2012), World Lakes Database, Japan. [Available online at www.ilec.or.jp/database/afr/afr-16.html].

James, P., A. Stohl, N. Spichtinger, S. Eckhardt, and C. Forster (2004), Climatological aspects of the extreme European rainfall of August 2002 and a trajectory method for estimating the associated evaporative source regions, *Nat. Hazards Earth Syst. Sci.*, *4*, 733–746.

Joussaume, S., R. Sadourny, and C. Vignal (1986), Origin of precipitating water in a numerical simulation of the July climate, *Ocean-Air Inter.*, *1*, 43–56.

Jung, G., and H. Kunstmann (2007), High-resolution regional climate modeling for the Volta region of West Africa, *J. Geophys. Res.*, *112*, D23108, doi:10.1029/2006JD007951.

Kalnay, E., et al. (1996), The NCEP/NCAR 40-Year Reanalysis Project, *Bull. Am. Meteorol. Soc.*, *77*, 437–471.

Koster, R., J. Jouzel, R. Suozzo, and G. Russell (1986), Global sources of local precipitation as determined by the NASA/GISS GCM, *Geophys. Res. Lett.*, *13*, 121–124.

Kunstmann, H., and G. Jung (2007), Influence of soil-moisture and land use change on precipitation in the Volta Basin of West Africa, *Int. J. River Basin Manage.*, *5*, 9–16.

Lafore, J.-P., et al. (2011), Progress in understanding of weather systems in West Africa, *Atmos. Sci. Lett.*, *12*, 7–12, doi:10.1002/asl.335.

Mlawer, E. J., S. J. Taubman, P. D. Brown, M. J. Iacono, and S. A. Clough (1997), Radiative transfer for inhomogeneous atmospheres: RRTM, a validated correlated-k model for the longwave, *J. Geophys. Res.*, *102*(D14), 16,663–16,682.

Mohamed, Y. A., B. J. J. M. van den Hurk, H. H. G. Savenije, and W. G. M. Bastiaanssen (2005), Hydroclimatology of the Nile: Results from a regional climate model, *Hydrol. Earth Syst. Sci.*, *9*, 263–278.

Moufouma-Okia, W., and D. P. Rowell (2010), Impact of soil moisture initialization and lateral boundary conditions on regional climate model simulations of West African Monsoon, *Clim. Dyn.*, *35*, 213–229, doi:10.1007/s00382-009-0638-0.

National Climatic Data Center (2012), Global Historical Climatology Network (GHCN), *National Oceanic and Atmospheric Administration, US.* [Available online at http://climexp.knmi.nl/getstations.cgi].

Nicholson, S. E., et al. (2003), Validation of TRMM and other rainfall estimates with a high-density gauge dataset for West Africa. Part I: Validation of GPCC rainfall product and pre-TRMM satellite and blended products, *J. Appl. Meteorol.*, *42*, 1337–1354.

Numaguti, A. (1999), Origin and recycling processes of precipitating water over the Eurasian continent: Experiments using an atmospheric general circulation model, *J. Geophys. Res.*, *104*(D2), 1957–1972.

Paeth, H., et al. (2011), Progress in regional downscaling of west African precipitation, *Atmos. Sci. Lett.*, *12*, 75–82, doi:10.1002/asl.306.

Patricola, C. M., and K. H. Cook (2010), Northern African climate at the end of the twenty-first century: An integrated application of regional and global climate models, *Clim. Dyn.*, *35*, 193–212, doi:10.1007/s00382-009-0623-7.

Reisner, J., R. M. Rasmussen, and R. T. Bruintjes (1998), Explicit forecasting of supercooled liquid water in winter storms using the MM5 mesoscale model, *Q. J. R. Meteorol. Soc.*, *124*, 1071–1107.

Savenije, H. H. G. (1995), New definitions for moisture recycling and the relationship with land-use changes in the Sahel, *J. Hydrol.*, *167*, 57–78.

Sodemann, H. (2006), Tropospheric transport of water vapour: Lagrangian and Eulerian perspectives, PhD thesis, 246 pp., ETH 16623, Swiss Fed. Inst. of Technol., Zurich, Switzerland.

Sodemann, H., C. Schwierz, and H. Wernli (2008), Interannual variability of Greenland winter precipitation sources: Lagrangian moisture diagnostic and North Atlantic Oscillation influence, *J. Geophys. Res.*, *113*, D03107, doi:10.1029/2007JD008503.

Sodemann, H., H. Wernli, and C. Schwierz (2009), Sources of water vapour contributing to the Elbe flood in August 2002—A tagging study in a mesoscale model, *Q. J. R. Meteorol. Soc.*, *135*, 205–223, doi:10.1002/qj.374.

Stohl, A., and P. James (2004), A Lagrangian analysis of the atmospheric branch of the global water cycle. Part I: Method description, validation, and demonstration for the August 2002 flooding in Central Europe, *J. Hydrometeorol.*, *5*, 656–678.

Sylla, M. B., E. Coppola, L. Mariotti, F. Giorgi, P. M. Ruti, A. Dell'Aquila, and X. Bi (2010), Multiyear simulation of the African climate using a regional climate model (RegCM3) with the high resolution ERA-interim reanalysis, *Clim. Dyn.*, *35*, 231–247, doi:10.1007/s00382-009-0613-9.

Tchotchou, L. A. D., and F. M. Kamga (2010), Sensitivity of the simulated African monsoon of summers 1993 and 1999 to convective parameterization schemes in RegCM3, *Theor. Appl. Climatol.*, *100*, 207–220, doi:10.1007/s00704-009-0181-2.

Trenberth, K. E. (1999), Atmospheric moisture recycling: Role of advection and local evaporation, *J. Clim.*, *12*, 1368–1381.

van der Ent, R. J., H. H. G. Savenije, B. Schaefli, and S. C. Steele-Dunne (2010), Origin and fate of atmospheric moisture over continents, *Water Resour. Res.*, *46*, W09525, doi:10.1029/2010WR009127.

Wagner, S., H. Kunstmann, A. Bàrdossy, C. Conrad, and R. R. Colditz (2009), Water balance estimations of a poorly gauged catchment in West Africa using dynamically downscaled meteorological fields and remote sensing information, *Phys. Chem. Earth*, *34*, 225–235, doi:10.1016/j.pce.2008.04.002.

Xue, Y., et al. (2010), Intercomparison and analyses of the climatology of the West African Monsoon in the West African Monsoon Modeling and Evaluation project (WAMME) first model intercomparison experiment, *Clim. Dyn.*, *35*, 3–27, doi:10.1007/s00382-010-0778-2.